Nanoscale Visualization of Crystal Habit Modification by Atomic Force Microscopy

Guangzhao Mao,[†,‡] Lloyd Lobo,[§] Ray Scaringe,[§] and Michael D. Ward*[,†]

Department of Chemical Engineering and Materials Science, Amundson Hall, University of Minnesota, 421 Washington Ave SE, Minneapolis, Minnesota 55455, and Imaging Research and Advanced Development, Eastman Kodak Company, Rochester, New York 14650-1708

Received September 11, 1996. Revised Manuscript Received December 10, 1996[⊗]

Atomic force microscopy (AFM) studies of *N*-[4-[4-cyano-2-(2-furanylmethylene)-2,5-dihydro-5-oxo-3-furanyl]phenyl]-1-butanesulfonamide (**1**), a crystalline dye used in photographic film, are described. AFM of the largest crystal face of freshly cleaved blade-shaped crystals of **1** revealed molecular scale contrast with periodicity identical with the low-energy oleophilic (100) plane, and ledges oriented along [001] with step heights equal to the *a* lattice parameter, which corresponds to the height of single molecules of **1**. These features are consistent with the solid-state structure of the dye, which reveals a low-energy oleophilic (100) plane and strong intermolecular $\pi-\pi$ interactions along [001]. Real-time in situ AFM reveals that growth of **1** near equilibrium conditions proceeds by flow of the [001] ledges along the [010] direction, consistent with the relative surface energies of the crystal planes and a terrace−ledge−kink mechanism. Addition of an ionic octyl oligoether sulfate surfactant to the growth medium resulted in significant curvature of the ledge topography in a manner consistent with the formation of [010] ledges, suggesting attachment of surfactant molecules to higher energy {001} or {011} step planes. This is manifested in the suppression of the nucleation of **1**, and changes in the crystal habit of submicron crystals from needles to blocks due to inhibited growth along the otherwise fast growing [001] direction. These studies provide direct and rapid observation of the origins of crystal habit modification by molecular additives at the nanoscale level.

Introduction

Crystallization is a key unit operation for the separation and purification of numerous organic commodity and specialty chemicals. Many commercial crystallization processes aim to control crystal characteristics such as morphology, size, and polymorphism, as these characteristics can influence solid flow, solubility, filterability, mechanical properties, aggregation behavior, dispersability, color, and bioavailability.[1−3] Control of crystal properties is achieved commonly by adjusting processing parameters such as solvent, temperature, and convection, although these parameters are optimized typically in an empirical manner. However, molecular level strategies for controlling nucleation,[4−6] polymorphism,,[7−9] and crystal morphology,[10−17] of organic crystals have been devised recently. Morphology modification has been achieved by addition to growth media of molecular species capable of attaching to specific crystal faces, thereby altering relative growth rates of the crystal faces. The influence of molecular additives on crystal morphology, and the specific molecular recognition events responsible for their action, typically are deduced by inference through inspection of macroscopic crystals retrieved from the growth medium. Morphology modification also has been examined by computational methods.[18−23] The effect of

* To whom correspondence should be addressed.
† University of Minnesota.
‡ Current address: Department of Chemical Engineering and Materials Science, Wayne State University, 5050 Anthony Wayne Drive, Detroit, MI 48202.
§ Eastman Kodak Co.
⊗ Abstract published in *Advance ACS Abstracts,* February 1, 1997.

(1) Carstensen, J. T. *Pharmaceutics of Solids and Solid Dosage Forms*; John Wiley and Sons: New York, 1977.
(2) Byrn, S. R. *Solid-State Chemistry of Drugs*; Academic Press, Inc.: New York, 1982.
(3) McKay, R. B., *Technical Applications of Dispersions*; Marcel Dekker, Inc.: New York, 1994; p 151.
(4) (a) Heywood, B. R.; Mann, S. *J. Am. Chem. Soc.* **1992**, *114*, 4681. (b) Popovitz-Biro, R.; Lahav, M.; Leiserowitz, L. *J. Am. Chem. Soc.* **1991**, *113*, 8943. (c) Landau, E. M.; Wolf, S. G.; Levanon, M.; Leiserowitz, L.; Lahav, M.; Sagiv, J. *J. Am. Chem. Soc.* **1989**, *111*, 1436.
(5) Campbell, A.; Fryxell, G. E.; Graff, G. L.; Reike, P. C., Tarasevich, B. *J. Scanning Microsc.* **1993**, *7*, 423.
(6) Frostman, L. M., Bader, M.; Ward, M. D. *Langmuir* **1994**, *10*, 576.
(7) Carter, P. W.; Ward, M. D. *J. Am. Chem. Soc.* **1994**, *116*, 769.
(8) Bonafede, S. J.; Ward, M. D. *J. Am. Chem. Soc.* **1995**, *117*, 7853.
(9) Hillier, A. C.; Maxson, J. B.; Ward, M. D. *Chem. Mater.* **1994**, *6*, 2222.
(10) Addadi, L.; Berkovitch-Yellin, Z.; Weissbuch, I.; van Mil, J.; Shimon, L. J. W.; Lahav, M.; Leiserowitz, L. *Angew. Chem., Int . Ed. Engl.* **1985**, *24*, 466.
(11) Berkovitch-Yellin, Z.; van Mil, J.; Addadi, L.; Idelson, M.; Lahav, M.; Leiserowitz, L. *J. Am. Chem. Soc.* **1985**, *107*, 3111.
(12) Black, S. N.; Williams, L. J.; Davey, R. J.; Moffat, F.; McEwan, D.; Sadler, D. E.; Docherty, R.; Williams, D. J. *J. Phys. Chem.* **1990**, *94*, 3223.
(13) Clydesdale, G.; Roberts, K. J.; Docherty, R. *J. Cryst. Growth* **1994**, *135*, 331.
(14) Clydesdale, G.; Roberts, K. J.; Docherty, R. *J. Cryst. Growth* **1994**, *141*, 443.
(15) Hanein, D.; Geiger, B.; Addadi, L. *Langmuir* **1993**, *9*, 1058.
(16) Hanein, D.; Geiger, B.; Addadi, L. *Science* **1994**, *263*, 1413.
(17) Markman, O.; Elias, D.; Addadi, L.; Cohen, I. R.; Berkovitch-Yellin, Z. *J. Cryst. Growth* **1992**, *122*, 344.
(18) Bennema, P. Morphology of Crystals, Past and Future. In *Science and Technology of Crystal Growth*; van der Eerden, J. P., Bruinsma, O. S. L., Eds.; Kluwer Academic Publishers: Boston, MA, 1995; p 149.
(19) (a) Hartman, P.; Perdok, W. G. *Acta Crystallogr.* **1955**, *8*, 49. (b) Hartman, P.; Perdok, W. G. *Acta Crystallogr.* **1955**, *8*, 521. (c) Hartman, P.; Perdok, W. G. *Acta Crystallogr.* **1955**, *8*, 525.
(20) Berkovitch-Yellin, Z. *J. Am. Chem. Soc.* **1985**, *107*, 8239.

S0897-4756(96)00470-X CCC: $14.00

molecular additives on morphology typically is considered to stem from attachment of the additive to the crystal plane of an actively growing face, producing a defect that acts either as a "blocker" (if the additive adsorbs on or is incorporated into the surface plane so that it protrudes from the interface) or as a "disruptor" (if it is incorporated into the surface plane so as to leave a pseudo-vacancy). The growth inhibition in each case results from a decrease in the energy released upon addition of the next plane of molecules, commonly referred to as a "slice." The role of solvent in determining crystal morphology has been examined,[24−27] but a universal model for the role of solvent has remained elusive.

We previously reported[28−32] that the nucleation and growth of organic and protein crystals can be visualized directly in growth media by atomic force microscopy (AFM).[33] Studies performed near equilibrium revealed that crystal growth occurred by a terrace−ledge−kink (TLK) mechanism,[34] which involves a series of elementary steps, including surface diffusion of molecules or aggregates and their attachment to terraces, ledges, or kinks.[35,36] The distribution and reactivity of these topographic features during the growth process were probed directly with AFM. These features could be correlated with the strength of intermolecular interactions along specific crystallographic directions and with the corresponding surface energies of the exposed terrace, step, and kink planes. The capabilities of the AFM to image topographic features under growth conditions provide an opportunity to examine the interaction between additives and well-defined nanometer scale crystal sites, thereby providing direct insight into the molecular-level origins of additive-induced habit modification. In this respect, AFM can provide better statistics with respect to the influence of additives as a large number of nanoscale features and events can be observed in a single experiment, compared to ex situ inspection of a limited number of mature crystals.

We describe herein AFM investigations of the nucleation and growth of *N*-[4-[4-cyano-2-(2-furanylmethylene)-2,5-dihydro-5-oxo-3-furanyl]phenyl]-1-butanesulfonamide (**1**), a crystalline dye employed in one of the optical filter layers of photographic film. Crystals of **1** tend to grow with a bladelike habit, which is undesirable for mass flow characteristics and filterability of aqueous dispersions of these crystals. To ensure uniform distribution of dye in the film matrix and avoid undesirable light diffraction, crystal growth and aggregation in the matrix must be suppressed so that crystal size is <250 nm. This typically is accomplished by the addition of surfactants to the crystallization medium and film matrix. These crystals are usually milled and dispersed in an aqeous medium to facilitate their incorporation into a film matrix, with a surfactant added to stabilize the colloidal dispersion. It is also reasonable to suggest that the surfactant can alter the growth modes of crystals of **1** by selective adsorption on different crystal planes. The particular surfactant used in the studies described here was an anionic octylphenyl oligoether sulfate (**2**). AFM provides direct observation of the influence of this surfactant on nucleation and growth at the nanometer level, providing molecular-level insight into the mechanism of specific additive binding to actively growing crystal planes.

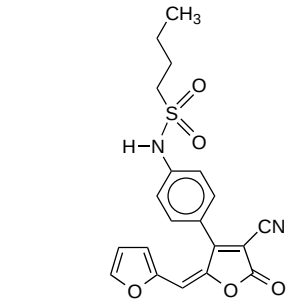

1

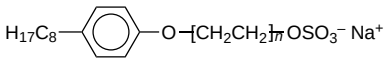

2 (*n* = 3–5)

Experimental Section

Materials. Single crystals of *N*-[4-[4-cyano-2-(2-furanylmethylene)-2,5-dihydro-5-oxo-3-furanyl]phenyl]-1-butanesulfonamide ($C_{20}H_{18}N_2O_5S$) were grown by cooling a saturated 2-propanol solution from 60 °C to room temperature, followed by slow evaporation of the solvent. The solubility of **1** in 2-propanol is 0.01255 mol/L at room temperature. Compound **1** crystallizes into needle-shaped thin plates, typically with lengths of about 2 mm. The sodium salt of octylphenyl polyether sulfonate was used as obtained (TX200, Eastman Kodak Co.) as a 6.8 wt % aqueous solution. 2-Propanol was used as obtained (EM Science HPLC grade).

Atomic Force Microscopy (AFM). AFM experiments were conducted with Digital Instruments Nanoscope III at room temperature in both air and in a liquid medium, using minimum forces in order to minimize damage to the samples. Si_3N_4 integral tips with a spring constant of 0.22 N/m were used in conjunction with a scan head with a maximum scan range of 14.6 × 14.6 μm^2 for both micron scale and high-resolution imaging. The scanner was calibrated with highly oriented pyrolytic graphite (HOPG) and muscovite mica. In situ AFM studies of dye crystal nucleation and growth were conducted in a commercially available cell designed for contact mode operation in liquid medium (Digital Instruments, Inc). Micron scale AFM images were acquired using either contact

(21) Docherty, R.; Clydesdale, G.; Roberts, K. J.; Bennema, P. *J. Appl. Phys. D.* **1991**, *24*, 89.
(22) Clydesdale, G.; Roberts, K. J.; Lewtas, K. *Mol. Cryst. Liq. Cryst.* **1994**, *248*, 243.
(23) Clydesdale, G.; Roberts, K. J. In *Science and Technology of Crystal Growth*; van der Eerden, J. P., Bruinsma, O. S. L., Eds.; Kluwer Academic Publishers: Boston, MA, 1995; p 179.
(24) Wang, J.-L.; Leiserowitz, L. Lahav, M. *J. Phys. Chem.* **1992**, *96*, 15.
(25) Davey, R.; Milisavljevic, Bourne, J. R. *J. Phys. Chem.* **1988**, *92*, 2032.
(26) Wireko, F. C.; Shimon, L. J. W.; Frolow, F.; Berkovitch-Yellin, Z.; Lahav, M; Leiserowitz, L. *J. Phys. Chem.* **1987**, *91*, 472.
(27) Davey, R. J.; Black, S. N.; Logan, D.; Maginn, S. J.; Fairbrother, J. E.; Grant, D. J. W. *J. Chem. Soc., Faraday Trans.* **1992**, *88*, 3461.
(28) Hillier, A.; Ward, M. D. *Science* **1994**, *268*, 1261.
(29) Carter, P. W.; Hillier, A.; Ward, M. D. *J. Am. Chem. Soc.* **1994**, *116*, 944.
(30) Hillier, A. C.; Maxson, J. B.; Ward, M. D. *Chem. Mater.* **1994**, *6*, 2222.
(31) Yip, C. M; Ward, M. D. *Biophys. J.* **1996**, *71*, 1071.
(32) Last, J. A.; Ward, M. D. *Adv. Mater.* **1996**, *8*, 730.
(33) Binnig, G.; Quate, C. F.; Gerber, Ch. *Phys. Rev. Lett.* **1986**, *56*, 930.
(34) Tiller, W. A. *The Science of Crystallization: Microscopic Interfacial Phenomena*; Cambridge University Press: New York, 1991; pp 327−381.
(35) (a) Bennema, P.; Gilmer, G. In *Crystal Growth: An Introduction*; Hartman, P., Ed.; North-Holland: Amsterdam, 1973; p 272. (b) Elwenspoek, M.; Bennema, P.; van der Eerden, J. P. *J. Cryst. Growth* **1987**, *83*, 297. (c) Bennema, P.; van der Eerden, J. P. In *Morphology of Crystals*; Terra Scientific Publishing Co.: Tokyo, 1987; pp 1−75. (d) Bourne, J. R.; Davey, R.; *J. Cryst. Growth* **1976**, *36*, 278. (e) Bourne, J. R.; Davey, R. *J. Cryst. Growth* **1976**, *36*, 287.
(36) Hartman, P. In *Crystal Growth: An Introduction*; Hartman, P.; Ed.; North-Holland: Amsterdam, 1973; p 367.

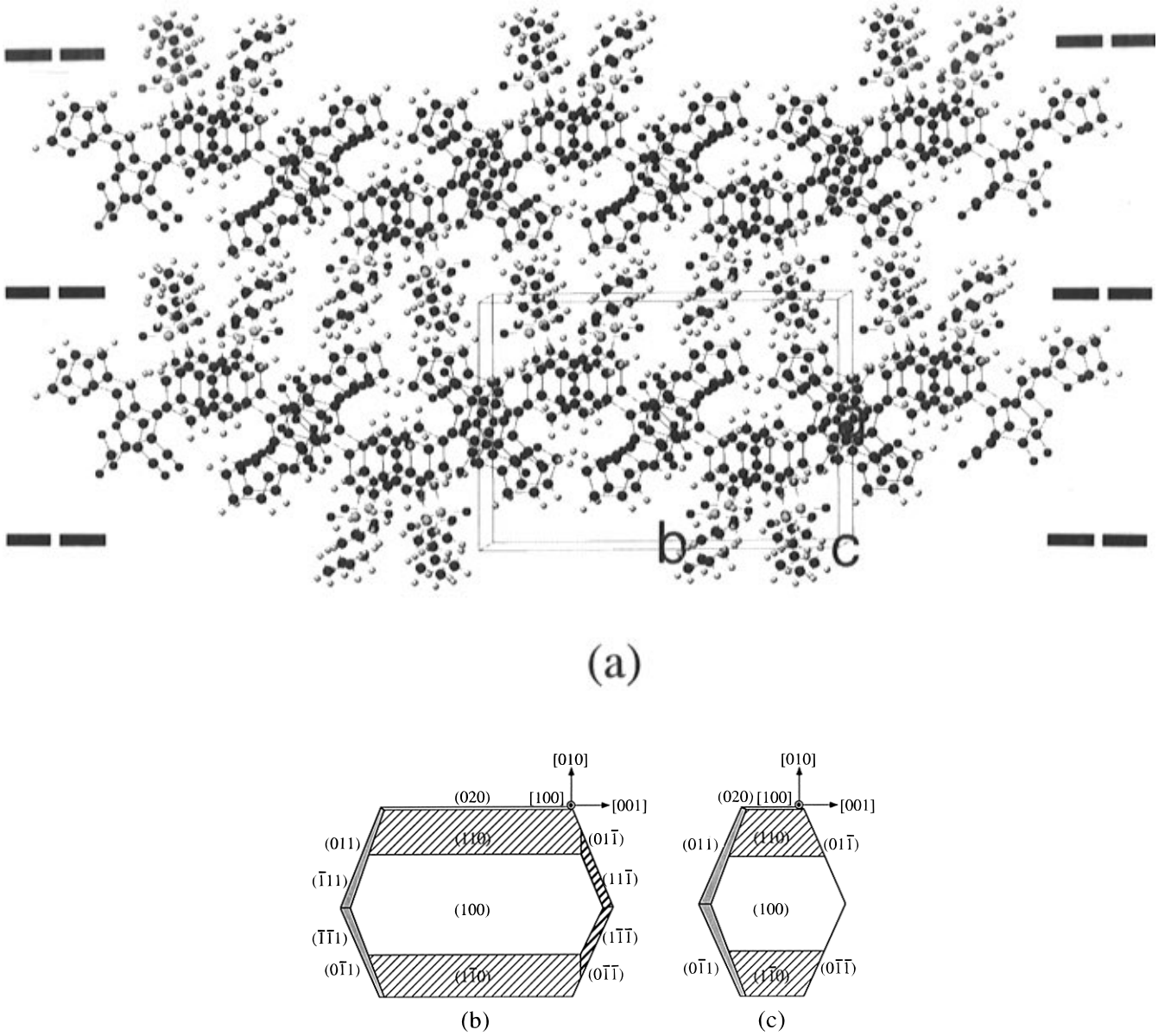

Figure 1. (a) Solid-state packing of **1** as viewed along the *c*-axis. The dashed markers indicate the regions of interdigitated butyl groups. (b) Calculated morphology of (**1**) as viewed along the [100] direction. The MI decreases in the order (100) > (110) > (010) > (011) > (111). This habit is similar to that observed for crystals grown from 2-propanol. (c) Calculated morphology of (**1**) for which the attachment energy of the (011) surface is reduced by a factor of 2 from that in (b). The MI decreases in the order (011) > (100) > (110) > (020) with values of 3.0, 2.6, 1.1, and 1.0, respectively (normalized to the smallest MI).

or tapping mode. AFM characterization of single crystals of **1** was performed on crystals which were mounted on a stainless steel disk such that the flat (100) face of the crystal was exposed. Freshly cleaved surfaces of these crystals were produced by removing surface layers of mounted crystals with adhesive tape. Crystal growth on the (100) face was studied directly in the AFM cell by adding a 2-propanol solution saturated with **1** to the AFM cell, which contained the affixed single crystal. Growth commenced shortly afterward when supersaturation was achieved by a small amount of solvent evaporation. Solutions were replenished periodically with fresh supersaturated solution if extended studies were performed. The influence of the surfactant **2** on crystal growth was examined by adding a 2-propanol solution saturated in **1** and containing 10^{-3} M **2**.

Molecular modeling and graphics were performed with the Computer Aided Chemistry (CAChe) molecular modeling program. Crystal morphologies and attachment energies were calculated with the Cerius[2] molecular modeling program, version 1.6 (Molecular Simulations Inc.), using the Bravais–Freidel–Donnay–Harker[37] routines and energy attachment modules, the latter employing a universal force field.[38] Two-dimensional Fourier transforms of crystal planes were calculated using Spyglass Transform (Spyglass, Inc., Savoy, IL).

Results and Discussion

Bulk Crystal Lattice Structure. The yellow dye *N*-[4-[4-cyano-2-(2-furanylmethylene)-2,5-dihydro-5-oxo-3-furanyl]phenyl]-1-butanesulfonamide (**1**) can be crystallized as small blade-shaped plates from 2-propanol. Single-crystal X-ray diffraction reveals that **1** crystallizes in the monoclinic space group $P2_1/c$, with a = 12.972 Å, b = 18.908 Å, c = 7.904 Å, and β = 94.70° (Figure 1).[39] Molecules of **1** are organized into stacks

(37) Reference to BFDH model. The MI values for the five planes with largest areas, normalized to the smallest plane, were (100) = 16.5, (110) = 10.1, (010) = 8.6, (011) = 8.3, (111) = 1.

(38) Rappe, A.; Casewit, C.; Colwell, K.; Goddard, W.; Skiff, W. *J. Am. Chem. Soc.* **1992**, *114*, 10024.

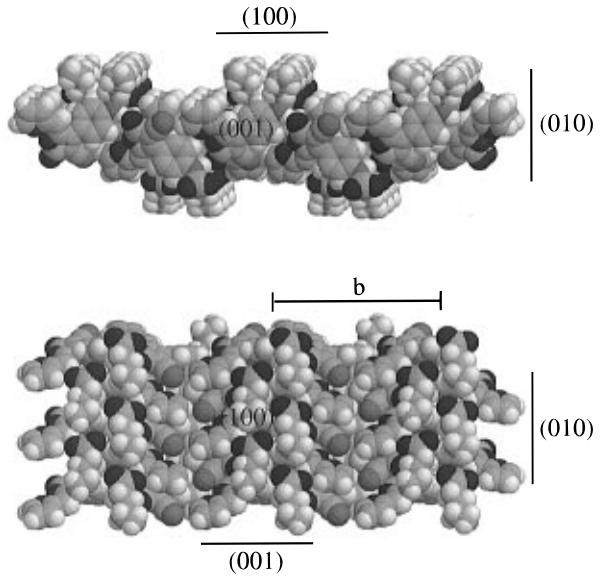

Figure 2. Space-filling model of the crystal structure of **1** illustrating the (100) as viewed nearly normal to (a) [001] and (b) [100] directions. The models shown have dimensions of $2a \times 2b \times c$.

along the *c* axis due to $\pi-\pi$ interactions between the phenyl and furanyl rings. The (100) plane consists of butyl and furan groups, with the former protruding from the plane in a manner that suggests that the (100) plane is a low surface energy oleophilic surface (Figure 2). The crystal organizes along the [100] direction by interdigitation of these butyl groups. Indexing revealed that the largest crystal face was (100) and that the needle axis was coincident with the [001] direction. This morphology is a consequence of the low surface energy of the (100) plane coupled with the high surface energy of the (001) plane because of truncated $\pi-\pi$ interactions. Consequently, growth in the [001] direction is fastest due to these interactions and the (001) face tends to grow out of existence. The weak van der Waals interactions between (100) planes also enable facile cleavage of the crystals so that pristine (100) faces can be prepared (vide infra). Morphology calculations based on energy attachment predicted a morphology resembling the observed one with the morphological importance (MI) decreasing in the order {100} > {110} > {010} > {011} > {111}. These calculations suggested that the tips of the crystals were composed primarily of {011} planes with smaller contributions from {111} planes.

Surface Topographical Features. AFM images acquired on the most prominent face of single crystals of **1** which had been retrieved from the 2-propanol crystallization liquor revealed rough surfaces with circular depressions having diameters ranging from 0.5 to 1 μm, which are attributed to dewetting during solvent evaporation (Figure 3a). The roughness of this surface prevented the acquisition of molecular contrast required for identification of the crystal face, although the morphology assigned by X-ray indexing indicates that it is the (100) face. These crystals could be cleaved by removing the surface layers with adhesive tape to generate freshly cleaved surfaces. AFM performed in air on these pristine faces revealed large terraces with prominent well-defined ledges oriented along two crystallographically different directions (Figure 3a). Attempts to obtain reproducible molecular contrast on these faces in air were thwarted by etching of the sample surface due to capillary effects and mechanical shear of the crystal surface by the AFM tip. The step height of these ledges was 13 Å, which was equal to d_{100} and consistent with the assignment of these faces as (100). One set of these ledges was assignable to [001] by comparison of its direction to the [001] direction of the indexed bulk crystal. The ledges of the other set subtend an angle of 20° ± 1.4° with respect to [001]. This suggested that these ledges correspond roughly with the [017] direction, but inspection of the solid-state structure of **1** did not reveal any single crystal plane capable of forming a step plane along this direction. The most likely explanation is that the [017] ledges are associated with vicinal steps that are composed of two different crystal planes. The formation of the [017] ledges instead of a parallel set of [001] ledges is curious. One possible explanation for the formation of high-energy ledges may be anisotropic stresses occurring during the cleaving process. The solid state structure and morphology calculations suggest that the two most likely step planes in this ledge are (010) and (011), the 20° angle requiring a (010):(01$\bar{1}$) composition ratio of approximately 2.5:1. Interestingly, the morphology calculations indicated that the MI ratio for these two planes was roughly 2:1, lending support to their role in forming the vicinal steps.

Addition of deionized water or saturated 2-propanol, directly in the AFM cell, to freshly cleaved crystals resulted in the complete disappearance of the [017] ledges so that only [001] ledges were evident. This was accompanied by the emergence of large (100) terraces. The disappearance of the [017] ledges is consistent with its high surface energy compared to the [001] ledges. Conversely, the larger areas observed for the (100) terraces are consistent with their low surface energy. While mechanical etching prevented the acquisition of molecular contrast in air, high-resolution AFM images of these (100) terraces were attainable in either deionized water or 2-propanol, revealing a periodic lattice with $b = 20.1$ Å, $c = 8.2$ Å, and $\alpha = 90°$ in water and $b = 19.5$ Å, $c = 8.3$ Å, and $\alpha = 90°$ in 2-propanol (Figure 3). The ability to obtain molecular contrast in liquid media can be attributed to reduced mechanical etching owing to the moderation of the tip−sample forces by the liquid medium.[40] Comparison of the 2-D unit cell orientation with crystal orientation, determined simultaneously with an optical microscope, revealed that the short axis of the 2-D cell was parallel to the needle axis of the crystal, assigned above to the [001] direction. The lattice parameters measured with AFM are identical, within experimental error, to the crystallographic values for the (100) plane ($b = 18.908$ Å, $c = 7.904$ Å, and $\alpha = 90°$). The 2-D Fourier transforms of images from both 2-propanol and water (Figure 3, insets) agreed with computer-generated Fourier transforms of the (100) plane. The images acquired in water exhibit contrast features consistent with butyl groups protruding from the surface (the brighter features in Figure 2a at the vertexes of the surface unit cell) and recessed furanyl

(39) The single-crystal X-ray structure of **1** was determined by J. Texter, L. Shuttleworth, and H. R. Luss (Kodak). The coordinates are available from the authors upon request.

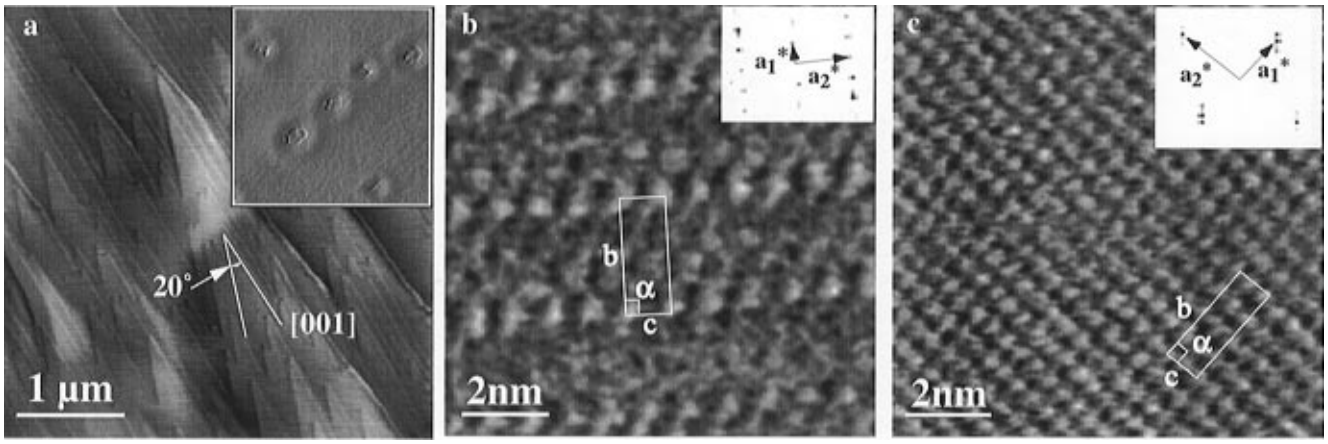

Figure 3. (a) AFM image of a freshly cleaved crystal **1** (100) surface in air revealing ledges along [001] and [017], subtending an angle of 20°. Inset: AFM image of the (100) surface of a single crystal **1** after retrieval from mother liquor and drying (image size is 4 μm × 4 μm). (b) High-resolution raw AFM data acquired in deionized water for a freshly cleaved (100) face of a single crystal of **1**. (c) High-resolution raw AFM data acquired in 2-propanol for a freshly cleaved (100) face of a single crystal of **1** . The unit cells depicted are consistent with the *bc* surface unit cell of **1**. The corresponding 2-D Fourier transforms of the data are depicted in the inset. The reciprocal lattice spacing, defined by a_1* and a_2* in the AFM data, correspond to the reciprocal lattice parameters b* and c* of crystalline **1**.

rings in the molecular troughs oriented along [001] which are formed by the double rows of butyl groups. However, the images in 2-propanol display a greater number of surface contrast features than the number of protruding butyl groups. The origin of this difference is not understood completely. It seems unlikely that the structure of the (100) plane would differ appreciably in these two solvents. AFM images can be deceiving as they represent a convolution of the sample surface and tip structure, but the differences illustrated by Figure 3 are representative of numerous samples and different tips. The increased number of contrast features observed in 2-propanol may reflect different ordering of the butyl groups on the exposed (100) surface, or possibly increased repulsive forces between the AFM tip and the [001] troughs, which are decorated with cyano functionalities. The latter may occur due to the lower dielectric constant of the 2-propanol solvent. The AFM contrast may also be due to rigid 2-propanol solvent molecules adsorbed in the [001] troughs, although such an observation would be highly unusual.

Atomic Force Microscopy of Nucleation and Growth. Previous AFM studies of organic crystals have revealed that crystal morphology is reflected in the nanoscale topography of selected crystal planes.[29] A similar correspondence between crystal morphology and topography also is evident in AFM images, acquired in 2-propanol, of the (100) face of single crystals of **1**. As mentioned above, these images revealed large (100) terraces, decorated with ledges predominantly oriented along the [001] direction. The predominance of the (100) terraces is consistent with a low surface energy for the (100) plane. It is presumed that the [001] ledges are formed from (010) planes, although the morphology calculations suggest that (110) and (1$\bar{1}$0) planes also are possible. Occasionally, AFM image frames exhibited ledges that were not perfectly linear along [001], suggesting contributions from other ledges, possibly [010]. Some of the nonlinear characteristics may be due partially to a scanning artifact associated with ledge motion that is faster than or comparable to the vertical velocity of the AFM tip[29] (the AFM image is acquired by the tip rastering horizontally across the imaged area with the tip moving vertically up or down after each raster line). Nevertheless, the infrequent appearance of features attributable to [010] ledges is consistent with the smaller MI of planes that would form these ledges. The MI of the (001) plane is neglible and no other (h0l) planes were apparent from the calculations. On the other hand, the appearance in the calculations of {011} planes, albeit with a small MI, suggests that ledges which appear to be oriented along [010] could result from equal areas of (011) and (0$\bar{1}$1) planes (or alternatively (01$\bar{1}$) and (0$\bar{1}\bar{1}$) planes). In this case the ledge actually would have an "accordion"-like structure.

Real-time AFM performed in 2-propanol solutions revealed that the [001] ledges advanced or receded in

(40) Hutter, J. L., Bechhoefer, J. *J. Appl. Phys.* **1993**, *73*, 4123. The resolution scale of AFM, RS, is determined by the area of contact between the tip and the sample, and therefore is determined by the short-range van der Waals force between the two surfaces.

$$\mathrm{RS} = \left(\frac{A_{132}R_0^{\,2}}{8KD_0^{\,2}}\right)^{1/3}$$

where R_0 and D_0 are the AFM tip radius and the minimum tip/surface separation allowed by repulsive contact forces, respectively, K is the combined elastic modulus of the tip/sample, and A_{132} is the Hamaker constant. According the above equation, the stronger the van der Waals attraction between the tip and the sample, the lower the AFM resolution becomes. Therefore, solvent media of different dielectric constants and refractive indices can be used to minimize the van der Waals attraction. The Hamaker constants in the relevant Si_3N_4/water/hydrocarbon and Si_3N_4/2-propanol/hydrocarbon were calculated based on a modified form of the Lifshitz equation

$$A_{132} = \frac{3}{4}kT\left(\frac{\epsilon_1 - \epsilon_3}{\epsilon_1 + \epsilon_3}\right)\left(\frac{\epsilon_2 - \epsilon_3}{\epsilon_2 + \epsilon_3}\right) + \frac{3h\nu}{8\sqrt{2}}\frac{(n_1^{\,2} - n_3^{\,2})(n_2^{\,2} - n_3^{\,2})}{(n_1^{\,2} + n_3^{\,2})^{1/2}(n_2^{\,2} + n_3^{\,2})^{1/2}[(n_1^{\,2} + n_3^{\,2})^{1/2} + (n_2^{\,2} + n_3^{\,2})^{1/2}]}$$

where A_{132} is the Hamaker constant between two surfaces of 1 and 2 in medium 3, and ϵ_n and n_n are the dielectric constants and refractive indices for the two surfaces 1 and 2 and medium 3; see: Israelachvilli, J. *Intermolecular and Surface Forces*, 2nd ed.; Academic Press: San Diego, CA, 1992. Based on values of $\epsilon_1 = 6.34$, $\epsilon_2 = 2.26$, $\epsilon_3 = 18.3$, $n_1 = 1.986$, $n_2 = 1.44$, $n_3 = 1.38$, the Hamaker constant for the van der Waals attraction between the silicon nitride tip and the hydrocarbon-rich dye (100) surface is 0.1154 eV in 2-propanol and 0.1752 eV in water. The better image quality in saturated 2-propanol solution is consistent with the smaller Hamaker constant in this solvent, which reduces the contact force so that better resolution and improved mechanical stability of the sample surface may be obtained.

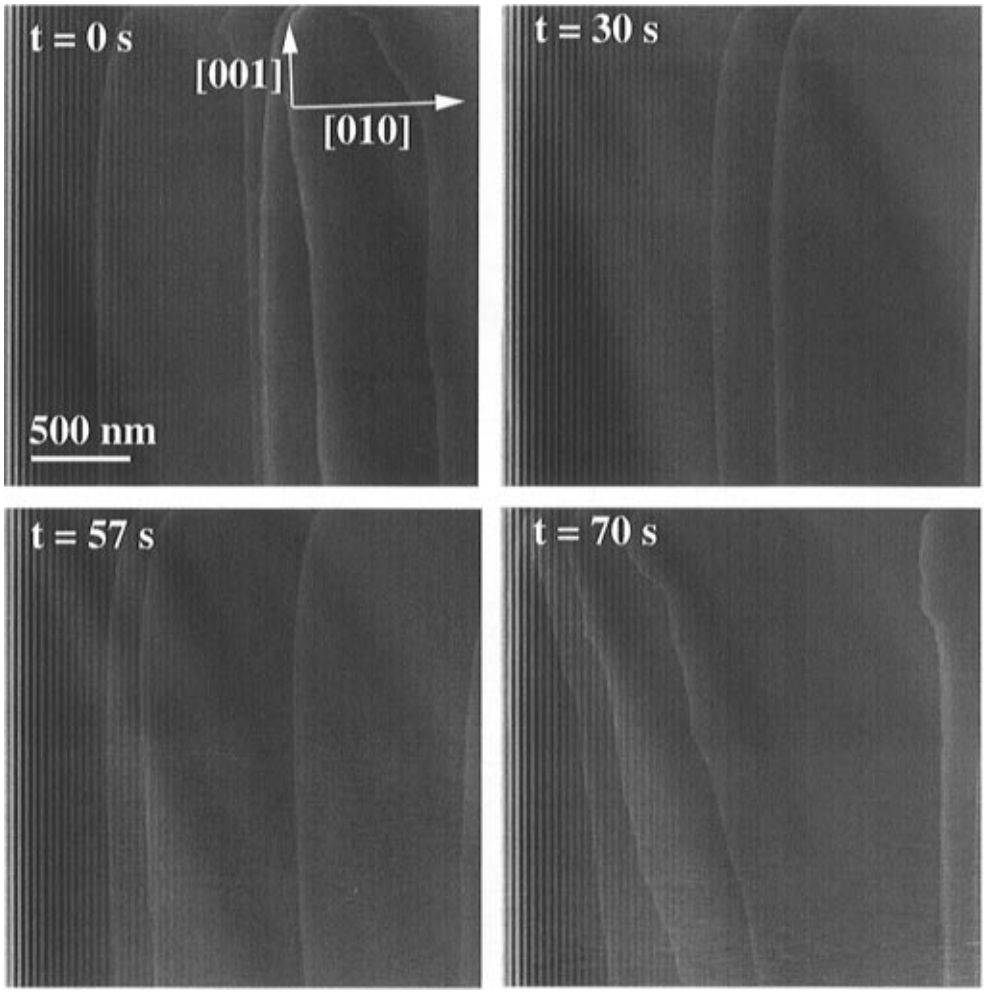

Figure 4. Sequential images of the (100) face of a single crystal of **1** obtained by real-time in situ AFM during crystal growth from 2-propanol solutions saturated with **1**. The (100) face exhibits large (100) terraces separated by steps along [001] ledges, which predominate under these conditions. Growth occurs by step flow along the [010] direction.

the direction of [010] in supersaturated or undersaturated solutions, respectively. These ledges exhibited negligible numbers of kink sites during growth, indicating that the high-energy planes that would necessarily comprise these features tended to grow out of existence very rapidly (Figure 4). Under typical growth conditions in saturated solutions, ledge motion was so rapid and the terraces so featureless that it was not possible to obtain ledge motion rates. This is consistent with very large surface energies for all crystal planes other than the oleophilic (100) plane. Nevertheless, the observed growth pattern is consistent with the conventional terrace−ledge−kink model (TLK), in which the growth modes are a manifestation of the relative surface energies of these nanoscopic features.[34] The terraces, which have the largest surface area owing to their low surface energy, are interrupted by ledges comprising the next lowest energy crystal plane. The TLK model invokes growth by attachment of molecules to a terrace surface, diffusion across the terrace, and attachment to the ledge, thereby generating a kink site. The large area of the terraces makes this sequence more probable than direct attachment to either ledges or kinks, although these direct processes cannot be totally excluded by the AFM data. Whereas attachment to terraces and ledge planes effectively raises the interfacial energy by creating a rougher surface, there is no net change in interfacial energy for attachment to kink sites as the number of new surfaces created is unchanged. Furthermore, the high surface energy of the kink plane generally is synonomous with strong intermolecular bonding along the direction normal to that plane, which will tend to increase the attachment rate. These factors conspire to favor rapid attachment to kink sites along the primary ledge. When this process is fast on the time scale of the AFM measurement, as is the case here for **1**, kinks are not observed readily as they rapidly grow out of existence. Rather, the rapid addition to kink sites along the primary ledge is observed as step motion perpendicular to the ledge. We note that scanning an area larger than a previously scanned area did not reveal any evidence for etching of these crystals by the AFM tip. Additionally, there was no evidence that the AFM tip inhibited or augmented growth in the scanned region.

The topography of the (100) surface of a single crystal of **1** changed considerably upon addition of the anionic octylphenyl oligoether sulfate surfactant **2** to the AFM cell containing saturated solutions of **1**. Immediately after addition of **2** the ledges became significantly "curved", suggesting substantially increased contributions from ledges with a component along the *b* axis, that is, along a [0*kl*] direction (Figure 5). The morphology calculations suggest that these ledges would comprise {011} or {111} planes, although the presence of (001) planes cannot be ruled out. These planes, and

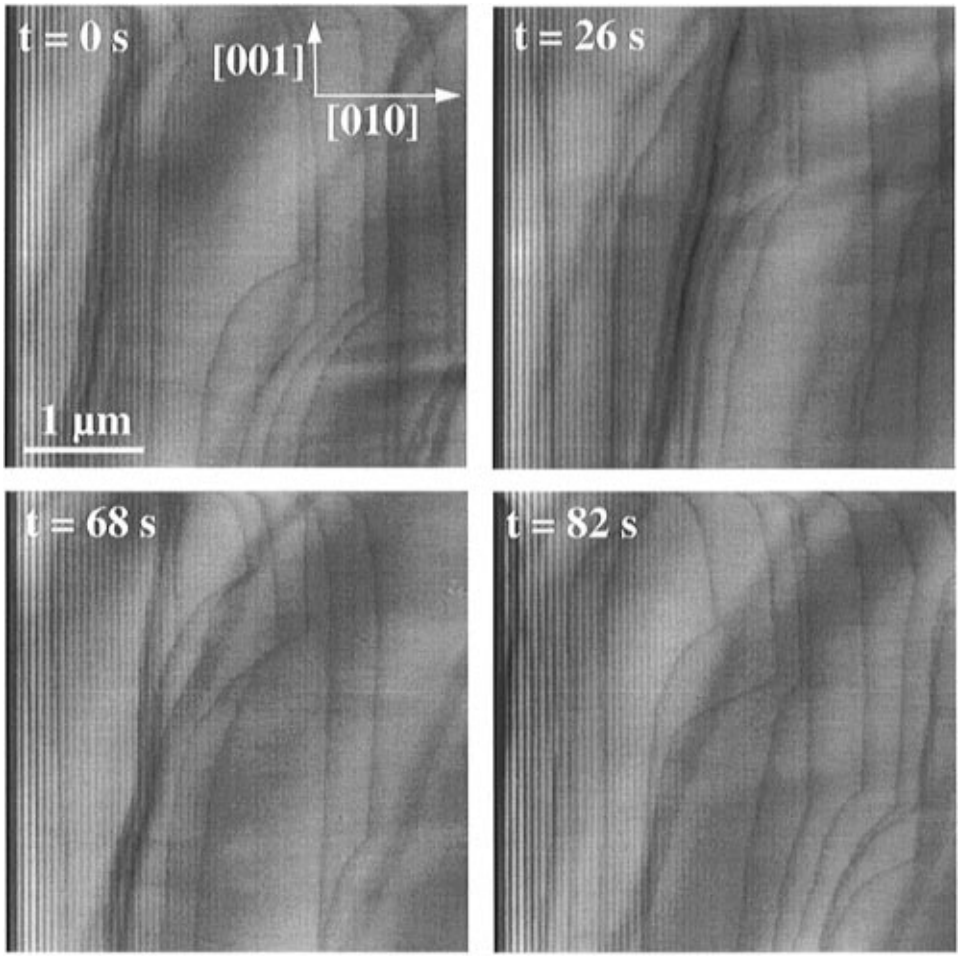

Figure 5. Sequential images of the (100) face of a single crystal of **1** obtained by real-time in situ AFM during crystal growth from 2-propanol solutions saturated with **1**, after addition of surfactant **2** ([**2**] = 1×10^{-3} M). The (100) face exhibits large (100) terraces separated by steps, but the ledges are curved in a manner which suggests the presence of [010] ledges in addition to [001] ledges. The curvature calculated from numerous AFM images corresponds to a ratio of [010]:[001] ledges of 0.12 ± 0.03.

their corresponding ledges, would become more prominent if surfactant molecules adsorbed in a manner that inhibited attachment of **1** to their surfaces. If only the principal lattice directions are considered, the observation of curved ledges is consistent with an increase in the growth rate along [010], relative to [001], compared to that in the absence of **2**. If the curved ledges are assumed to be composites of [001] and [010] oriented ledges, analysis of numerous AFM images reveals that the ratio of [010]:[001] ledges is 0.12 ± 0.03 in the presence of **2** compared to very small values in most image frames acquired in the absence of **2** (vide supra). These results indicate that **2** serves to block attachment of **1** to the high-energy planes responsible for growth along the *c*-axis. The influence of **2** was modeled qualitatively by morphology calculations in which it was assumed that **2** adsorbed to {011} planes on the [010] ledges. Comparison of the observed morphology to calculations suggested that the changes in the nanoscale topography could be realized if the surfactant adsorption resulted in a reduction of the (011) attachment energy by a factor of 2. The emergence of [010] ledges upon addition of surfactant is consistent with the change from a one-dimensional bladelike habit, resulting from growth predominantly along one crystallographic direction, to a blocklike habit resulting from growth along two directions (vide infra). This demonstrates that AFM can probe directly, and rapidly, the influence of molecular additives on crystal habit at the nanoscale level.

It is important to note that the surfactant **2** typically is used to stabilize colloidal dispersions of the filter dye **1**, which is essential to its performance in photographic film. This stabilization is surmised to occur by adsorption of the hydrophobic alkane tail **2** to the surface of the colloidal particles with the sulfonate groups extending from the surface, thereby preventing aggregation by electrostatic repulsion between the negatively charged ions. It is reasonable to speculate that this occurs by adsorption of the alkane tail on the oleophilic (100) plane of crystals of **1** (or colloidal particles with crystalline character) so that the negatively charged sulfonate groups remain extended outward from the crystal surface. Indeed, molecular models suggest that the molecular troughs defined by the butyl groups on the (100) plane provide ideal sites for alkane tail adsorption (Figure 6). Specific adsorption on the (100) face alone would lead to suppression of growth only along the [100] direction and to an increase in the area of the (100) terraces. However, this would be difficult to discern as the growth along [100] is slow and the (100) terrace area is large even in the absence of surfactant. In contrast, even a minor amount of adsorption of **2** onto step planes of the [010] ledge would alter the bulk crystal morphology and change, in a nearly instantaneous manner, the nanoscale surface topography observed by AFM. Adsorption of the alkane tail in the molecular troughs on the (100) face would not be expected to instigate the formation of [010] ledges, but molecular models indicate

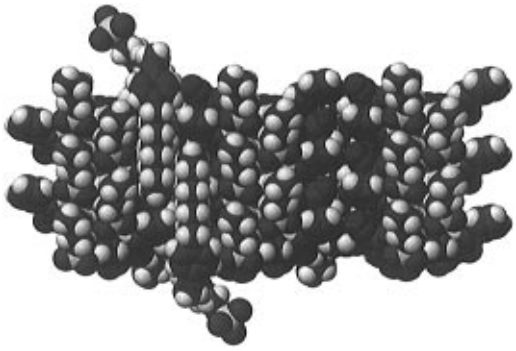

Figure 6. A space-filling model of **2** adsorbed on **1**. Two molecules of **2** are depicted here, adsorbed on the oleophilic (100) face nestled in the molecular troughs between the double rows of butyl groups protruding from this crystal plane. The headgroup containing the phenyl ring and the ethoxylated chain is brought into proximity with the (001) face. This can suppress growth along the (001) direction, while also allowing the sulfonate group to extend from the crystal surface so that aggregation is inhibited.

that this would bring the phenyl ring and the ethoxylated side chain into proximity with the high-energy step planes of the [010] ledge, shown by example in Figure 6 as the (001) plane. The mode of adsorption depicted in Figure 6 would enable the sulfonate group to remain extended from the crystal surface so that aggregation would be inhibited. While direct adsorption of the alkane tails onto the step planes of the [010] ledge cannot be eliminated, the model depicted in Figure 6 is appealing owing to the large area of the (010) terraces upon which the initial adsorption can occur.

Nucleation and Growth on Graphite. Nucleation and growth of **1** on a freshly cleaved, highly oriented pyrolytic graphite (HOPG) surface was examined in situ by injection of an 2-propanol solution saturated with **1** into an AFM cell containing a freshly cleaved HOPG substrate. HOPG was chosen as a substrate for these experiments as its atomic flatness would enable observation of monolayer-thick nuclei, and preliminary experiments indicated that the (100) face of **1** adhered to the HOPG surface with slight heating, suggesting favorable dispersive interactions. The latter suggested that nucleation of **1** may occur by the formation of (100) layers on this substrate. Shortly after introduction of

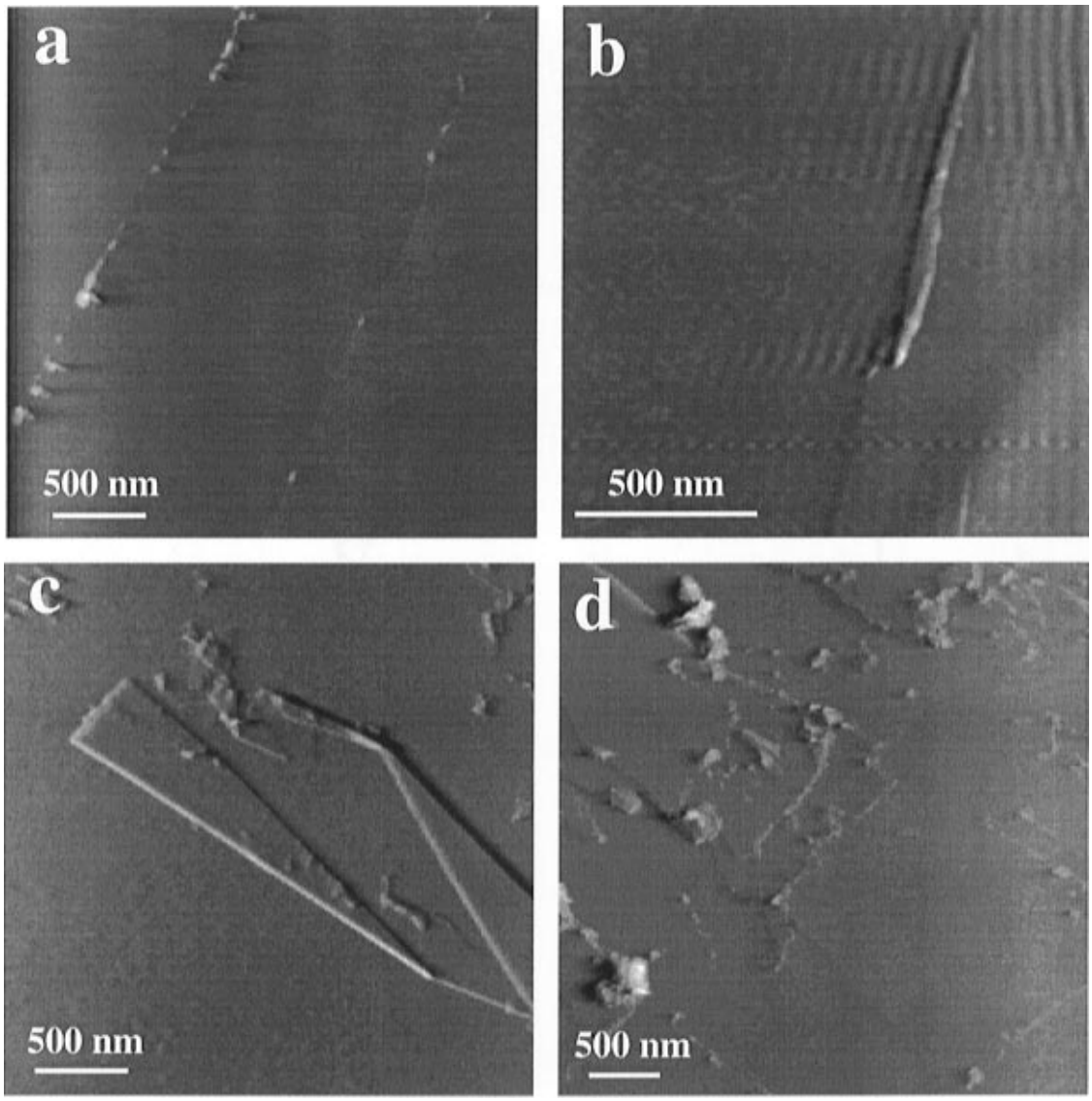

Figure 7. (a) Nucleation and growth of **1** from a 2-propanol solution at a dislocation on an HOPG substrate. (b) A needle-shaped crystal of **1** formed by coalesence of nuclei at a HOPG dislocation. (c) Formation of monolayer-thick crystals of **1** on the HOPG surface. Note the triangular habit with resembles the morphology of the terraces of freshly cleaved crystals illustrated in Figure 3. (d) A multilayer-thick film of **1** formed later in the growth process. Macroscopic crystals eventually grow from these films.

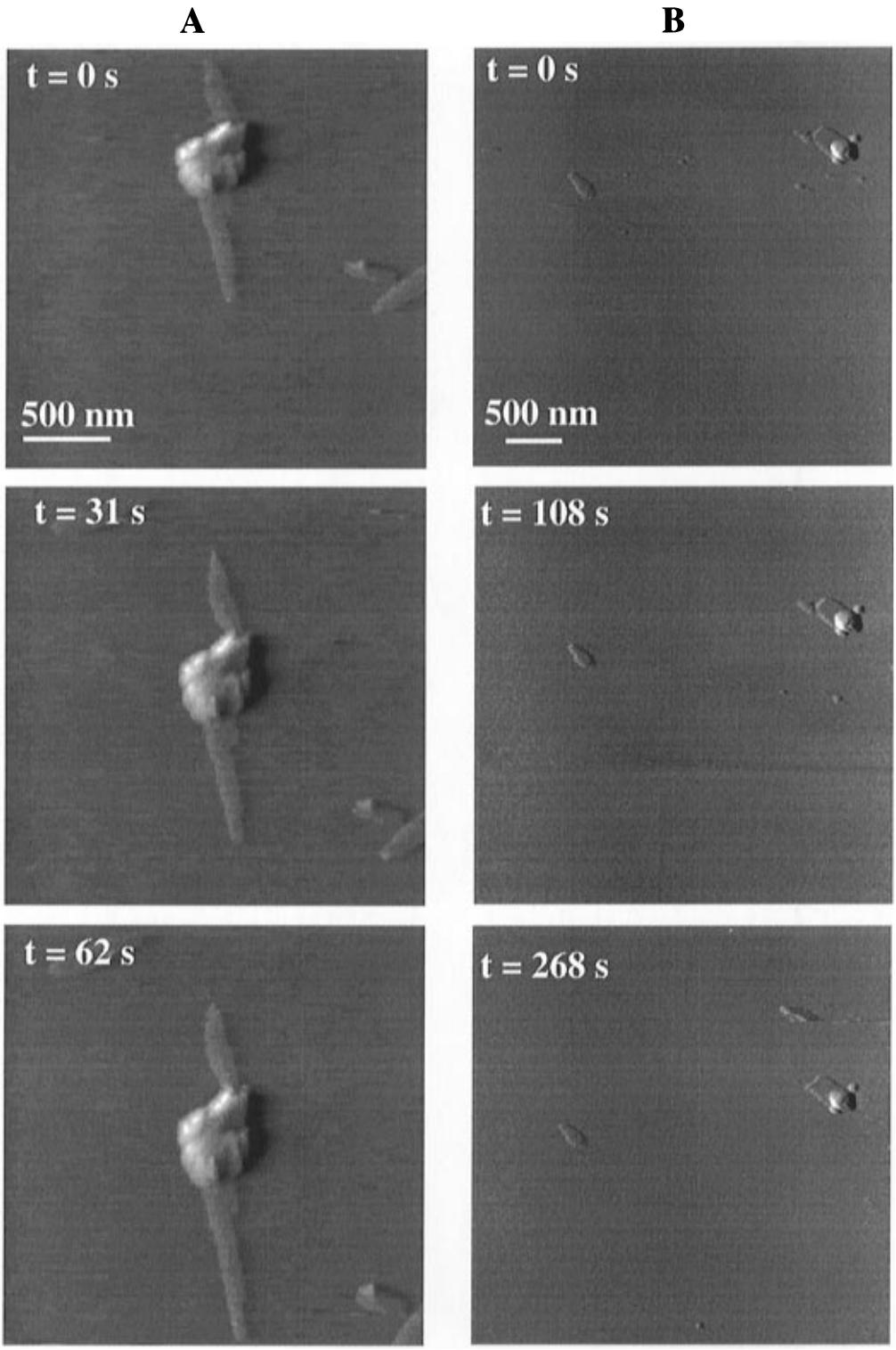

Figure 8. Series A: Typical growth behavior observed for **1** on a HOPG surface in saturated 2-propanol solution. Growth occurs by emergence of a needle-shaped front from a small aggregate of **1** illustrating the advancement of the needle tip over approximately one minute. Series B: Typical growth behavior under the same conditions as in Series A, but in the presence of surfactant **2**. The nucleation rates are substantially reduced and the needle-shaped growth fronts are absent. The crystals observed have a blocklike habit similar to the morphology calculated with reduced attachment energy for the (011) planes.

the saturated 2-propanol solution to the AFM cell, small clusters of **1** formed at steps present on the HOPG surface (Figure 7a,b). Nucleation from solutions that were not purposely supersaturated may be due to favorable heterogeneous nucleation on the HOPG substrate or to slight evaporative loss of solvent from the AFM cell. The clusters eventually coalesced into long needles, oriented along the HOPG steps, which grew longer with time but with negligible growth in other directions at short times. Occasionally, needle-shaped crystals emerged from cluster aggregates that had formed on the HOPG surface (Figure 8). Real-time measurements indicated that under these conditions the tips typically advanced at a rate of approximately 50 Å/s. Needles that had nucleated on HOPG steps eventually grew into well-defined flat plates having thicknesses of approximately 13 Å, equivalent to d_{100} (Figure 7c). This indicated that these plates were two-dimen-

sional crystals with a structure mimicking that of bulk crystals of **1**. Furthermore, in the early stages these two-dimensional crystals exhibited a triangular morphology resembling that of the features observed on the surface of a freshly cleaved crystal of **1**. We presume this is due to formation of a molecular ledge along the *c*-axis and a molecular ledge with vicinal-like character along a higher index direction. The angle subtended by the two ledges in the two-dimensional crystals is slightly smaller than that on the cleaved surface (12−15°) but this may be due to these ledges being generated during the growth phase in a solvent medium, which can alter the surface energetics compared to the cleaved crystals. Nevertheless, this suggests that these two-dimensional crystals mimic the bulk crystal with respect to the surface energy of molecular planes as well as their crystal structure. Further growth resulted in the formation of multiple layers of **1** from these triangular crystals, with the multilayers covering the entire HOPG surface. Steps between different layers exhibited heights equal to d_{100}. Bulk crystals of **1** eventually grew from the these layers provided the concentration of the solution was maintained above saturation. The crystals were oriented with their *a*-axis normal to the HOPG surface, as verified by high-resolution AFM. This indicated that the bulk crystal orientation was dictated by the initial nucleation events on the HOPG surface. The observed growth behavior is that expected based on simple free energy considerations as the two-dimensional crystals and films are oriented so that the strongest intermolecular bonding is in the plane parallel to the substrate and the weakest intermolecular bonding, and correspondingly the lowest surface energy, is normal to the substrate.

The observation of heterogeneous nucleation of **1** on the HOPG substrate suggests the presence of favorable interactions between **1** and the substrate that enables nucleation from solutions that, at least initially, were not supersaturated. Calculations performed with a custom-made program written in our laboratory capable of searching for epitaxial relationships found no suitable two-dimensional epitaxy that may drive the formation of (100) layers on the HOPG substrate.[41] Rather, the evidence suggests that growth occurs from nuclei formed on the HOPG dislocation ledges with nonspecific wetting of the HOPG surface by the two-dimensional crystals of **1**. The (100) orientation most likely dominates because of its low surface energy and stronger in-plane bonding compared to other planes. Identical experiments performed with hydrophilic mica substrates revealed no significant growth of **1** from 2-propanol solutions during the typical time of an AFM experiment. This suggests either a smaller defect density on the mica surface compared to that of graphite or poor wetting of the two-dimensional nuclei on the polar mica surface.

When the crystallization of **1** was examined by AFM with an HOPG substrate under conditions identical with those described above but in the presence of a small amount of **2**, the number of crystals formed on the HOPG surface was reduced substantially. The time required for the formation of these small prismatic crystals was substantially longer than in the absence of surfactant. Furthermore, the crystals were small prisms instead of the needles observed in the absence of **2**. These observations indicate that heterogeneous nucleation was suppressed by **2** and that the morphology was altered substantially in a manner consistent with **2** preventing the attachment of solute to {001} faces, as described earlier. The attachment of **2** to faces normal to the fast-growing [001] direction would inhibit crystal growth significantly. It also should be noted that it is possible that the surfactant alkane tail adsorbs to the HOPG surface such that the hydrophilic headgroups are present at the growth interface. Given the absence of growth on mica surfaces, such a surface could limit heterogeneous nucleation.

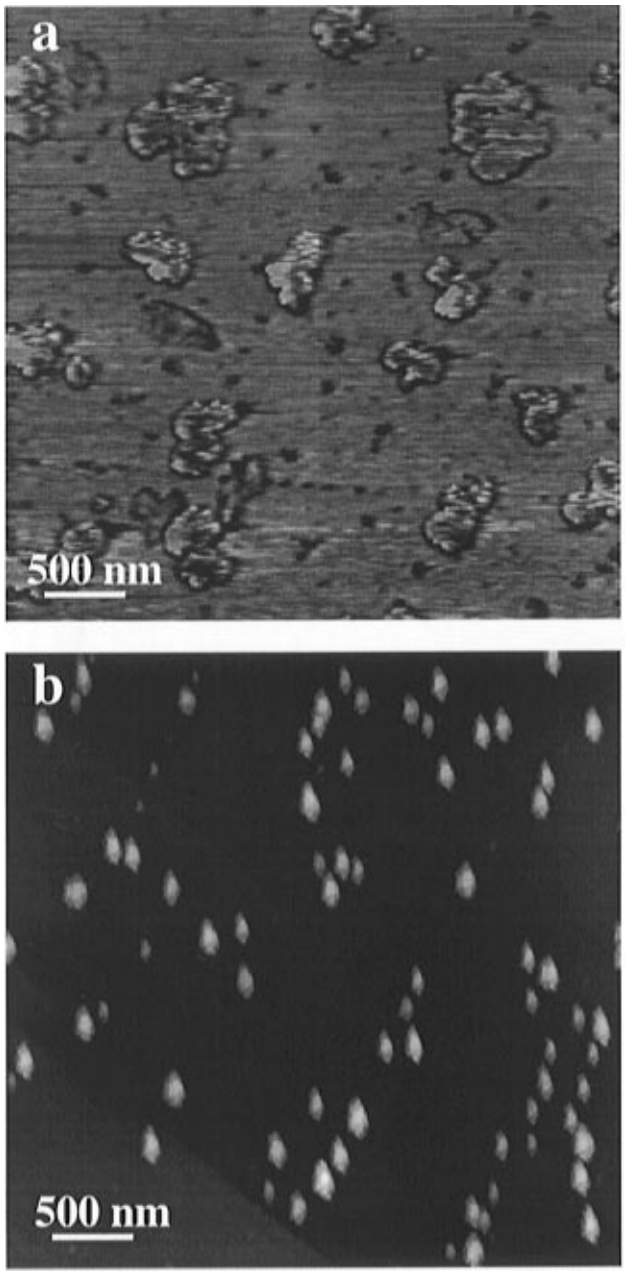

Figure 9. AFM images of particles of **1** obtained by drying aqueous dispersions (a) without **2** and (b) with **2**. The reduction of aggregation in the presence of the surfactant is evident.

The filter dye **1** is customarily stored in an aqueous dispersion after milling. To estimate dispersion particle size distribution and to image particle morphology simultaneously, drops of a dilute sonicated suspension

(41) The custom-made program for analysis of epitaxy, EpiCalc, runs in the Microsoft Windows environment on a 486 processor and is available on the World Wide Web at http://www.cems.umn.edu/research/ward.

of **1** were placed on a graphite substrate. The solvent was removed by evaporation under gentle heating and AFM was used to analyze the particle sizes and morphologies of the resulting graphite-bound dye particles. Samples prepared in this manner in the absence of **2** revealed ill-defined aggregates with an average particle size of 0.3 μm^2 (Figure 9). In the presence of **2**, the particles exhibited distinct and uniform crystal morphology and an average particle size of 0.004 μm^2. These observations also are consistent with adsorption of **2** on the surfaces of particles of **1**, with electrostatic repulsive force preventing coagulation. X-ray powder diffraction patterns for crystals grown in the absence and presence of **2** were identical, eliminating the possibility of differing particle attributes due to polymorphism. Rather, these experiments clearly indicate that **2** is an effective stabilization agent for dispersions of **1**.

Conclusions

The observations described above reveal that influence of molecular additives on crystal morphology can be probed at molecular level in real time under actual growth conditions using atomic force microscopy. These studies indicate that an ionic amphiphile known to stabilize colloidal dispersions of an important photographic dye alters the nanoscopic topography of the crystal face upon which growth occurs. The surfactant induces the formation of ledges which must contain higher energy crystal planes, consistent with adsorption of the surfactant on a crystal plane oriented normal, or nearly normal, to the otherwise fast growing direction. Analysis of the influence of molecular additives on morphology using AFM provides substantially more data than can be realized by examining the habit of mature crystals harvested from the crystallization medium. This not only provides for better statistics concerning the influence of the additive but it also enables immediate observation of morphology changes induced by molecular additives directly in the AFM cell. The studies described here reveal that the influence of a molecular additive on crystal growth, as observed by AFM, is consistent with its influence on the habit of bulk crystals. We anticipate that similar investigations performed on other crystalline materials can provide substantial insight into nucleation and growth and can facilitate optimization of crystallization processes.

Acknowledgment. This work was supported by the National Science Foundation and the Center for Interfacial Engineering, a National Science Foundation Energy Research Center. The authors also acknowledge J. Texter, L. Shuttleworth, and H. R. Luss (Eastman Kodak Co.) for providing the structural coordinates for **1**.

CM960470L